Effect of barrier layer on moisture absorption of thin carbon-fiber-reinforced plastic mirror substrates

Hisamitsu Awaki
Tessei Yoshida
Chisato Oue
Nozomi Aida
Hironori Matsumoto
Tomohiro Kamiya

Effect of barrier layer on moisture absorption of thin carbon-fiber-reinforced plastic mirror substrates

Hisamitsu Awaki,[a,*] Tessei Yoshida,[a,b] Chisato Oue,[a] Nozomi Aida,[a] Hironori Matsumoto,[c]
and Tomohiro Kamiya[d]
[a]Ehime University, Matsuyama, Ehime, Japan
[b]Comprehensive Research Organization for Science and Society, Shirakata, Tokai, Ibaraki, Japan
[c]Osaka University, Toyonaka, Osaka, Japan
[d]Japan Aerospace Exploration Agency, Sengen, Tsukuba, Ibaraki, Japan

Abstract. Carbon-fiber-reinforced plastic (CFRP) has a higher strength-to-weight ratio and forming flexibility than metals, making it suitable for fabricating lightweight x-ray mirrors. However, CFRP has the disadvantages of print-through and deformation due to moisture absorption, which have prevented its use in optical mirrors. To expand the application of CFRP, we studied the formation of a moisture barrier layer on CFRP substrates. We formed a flattening layer a few micrometers thick on a CFRP substrate, following which we coated the substrate with SiO_x as a moisture barrier. The effect of moisture absorption was then evaluated using accelerated aging tests. We found that the diffusivity of the CFRP substrate at 60°C and a relative humidity of 100% was $\sim 2 \times 10^{-6}$ mm^2 h^{-1}, which is 1/500th that of the barrier-less substrate. In the tests, the moisture absorption rate increased after $\sim$800 h. As we observed cracks on the flattening layer after 600 h, the rate increase could be associated with these cracks. Considering the damage to the barrier layer, we propose a modified model for the time profile, which is congruent with the observed time profile of the moisture content. © The Authors. Published by SPIE under a Creative Commons Attribution 4.0 Unported License. Distribution or reproduction of this work in whole or in part requires full attribution of the original publication, including its DOI. [DOI: 10.1117/1.JATIS.5.4.044001]

Keywords: x-ray optics; x-ray telescope; carbon-fiber-reinforced plastic.

Paper 19050 received May 9, 2019; accepted for publication Sep. 16, 2019; published online Oct. 8, 2019.

1 Introduction

With the advent of telescopes, it has become possible to detect weak light and detailed structures in the universe that cannot be observed by the human eye. In the x-ray band, many discoveries have been made using x-ray telescopes. Since x-ray optics work in grazing-incidence configuration, the effective area is much smaller than the surface area of the mirror. It is difficult to fabricate the mirrors that have both a high spatial resolution and a large effective area. The design of x-ray telescopes is roughly classified into two types based on the mirror configuration: one type focuses on achieving a high spatial resolution,[1–3] while the other focuses on achieving a large effective area.[4–12] To respond to recent scientific requirements, future large facilities such as Athena and Lynx should achieve an angular resolution much better than 30 arc sec [5 arc sec half-energy diameter (HED) for Athena,[13] 0.5 arc sec HED for Lynx[14]].

For developing a lightweight, high-throughput telescope with subarc min angular resolution, we study thin carbon-fiber-reinforced plastic (CFRP) mirror with the original monolithic Wolter-I geometry.[15–17] In our CFRP mirror, thin CFRP is used as the mirror substrate instead of the thin aluminum foil often used in the conventional lightweight telescopes such as ASCA XRT. A smooth surface on the CFRP substrate can be formed using a replication method.[15] CFRP has a low specific weight of $\sim$1.7, which is 0.6 times that of aluminum. Furthermore, the coefficient of elasticity of CFRP is 7 times that of aluminum, while its coefficient of thermal expansion is two orders lower than that of aluminum. Moreover, the forming flexibility of

CFRP makes it possible to form original monolithic Wolter-I substrates. The monolithic Wolter-I mirror has the advantage of reducing the degradation of image performance due to alignment errors, and the reduction of the alignment error is particularly important to manufacture a large-area telescope. However, there are known disadvantages of using CFRP as a substrate for high-precision optics[18–28] and, in particular, x-ray mirrors.[29] One is the microscale deformation of the substrate surface, which is called print-through. Print-through is caused by both the cure shrinkage of resin and the difference of thermal expansion coefficient between the resin and the carbon fiber. We previously demonstrated that it is possible to reduce the effect of print-through in the replication process.[30] Another disadvantage of CFRP is the long-term deformation resulting from the aging effect due to the swelling phenomenon. The swelling phenomenon is caused by moisture absorption, which originates from the resin. Sugita et al.[31] measured the deformation of a CFRP substrate after drying and moisture absorption and found that the history of drying and moisture absorption influence the deformation. Thus, it is crucial to make the change of the moisture content in CFRP small, in order to suppress the deformation. One method that reduces the effect of moisture absorption utilizes a barrier layer on the CFRP surface. We previously coated a thin CFRP substrate with functional sheets having a low water-vapor transmissivity and found that such coating is effective for reducing moisture absorption.[31]

Although it is easy to laminate a flat CFRP substrate with functional sheets, it might not be easy to laminate a CFRP substrate with a complex geometry, such as Wolter-I optics. Thus, in the present study, we coated a moisture barrier layer on the CFRP substrate, instead of using functional sheets, and evaluated its moisture absorption effect by using accelerated aging

tests. We previously found that the time profile of moisture absorption in a CFRP substrate with a barrier layer cannot be reproduced by a simple diffusion model.[31] To evaluate the effect of the moisture barrier, in the present study, a model characterizing the time profile of the moisture absorption is proposed to represent the time profile considering damage to the moisture barrier.

2 Fabrication of Carbon-Fiber-Reinforced Plastic Sample

2.1 Carbon-Fiber-Reinforced Plastic Substrate

In the fabrication of flat CFRP substrates for studying the moisture barrier, we utilized a prepreg sheet as the substrate material. Prepreg is a reinforcing fabric that has been preimpregnated with a resin. By including the proper curing agent for the resin, it is easy to fabricate the CFRP substrate by laying the prepreg into a mold and by applying pressure and heat to the laminate for curing. Commercial prepregs also have the advantages of uniformity and repeatability. We used the UD prepreg sheet for our experiment, which consists of high-elasticity-type pitch fibers with epoxy resin and is developed by Nippon Graphite Fiber (model no. E7026B-05S). The thickness of the prepreg is 50 μm. Table 1 lists the properties of the prepreg sheets. The molds for CFRP-forming are 10-mm-thick float-plate glasses that hold the prepreg sheets on the top and bottom sets. We adopted quasi-isotropic 8-ply lamination with the laminated constitution of [0/45/−45/90] s. Further details are described in our previous report.[31]

After laminating the prepreg sheets on the mold, we employed a vacuum-bagging method for applying pressure on the laminated prepreg. In this method, both the prepregs and the mold are bagged with seal film and pressed at atmospheric pressure. The laminate was cured for 3 h at 130℃ in the vacuum bag. The CFRP substrates were ∼100-mm wide, 100-mm long, and 0.38-mm thick.

2.2 Barrier Coating

We previously performed a precursor experiment for a moisture barrier in 2015.[31] In that experiment, both sides of a CFRP substrate were covered with a moisture barrier film, and it was noted that a moisture barrier film with low water-vapor transmissibility of <0.1 g · m^{-2} · day^{-1} showed high-barrier properties. In particular, a barrier film coated with SiO_x worked well. However, as mentioned previously, it would not be easy to deposit the film on a CFRP substrate with a complex geometry. Thus, in the present study, we performed barrier coating on the CFRP substrate instead of depositing a barrier film.

First, we performed direct SiO_x barrier coating on a CFRP substrate by conventional plasma chemical vapor deposition

Table 1 Properties of the prepreg sheets used in our experiment.

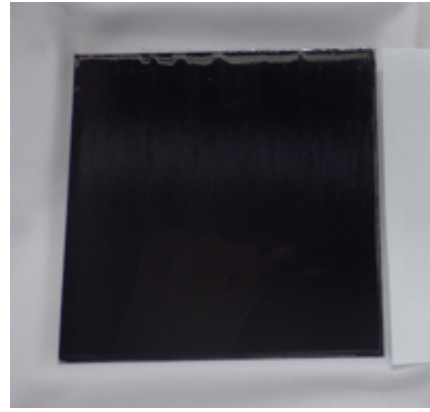| Model no.	E7026B-05S
Thickness	50 μm
Fiber	YSH-70A
Filament diameter	7 μm
Resin content	35%

Fig. 1 A picture of sample 2 (ID 180831). The size is 100-mm square.

method. In this method, the monomer gas (HMDSO) is decomposed in a vacuum chamber so that a thin SiO_x layer is formed on the CFRP. However, the coating did not work well, because a thin layer of SiO_x was not uniformly formed on the substrate owing to irregularities on the substrate. Next, we formed a flattening layer on the CFRP substrate prior to coating SiO_x on the CFRP substrate. We fabricated two samples, sample 1 (ID 180829) and sample 2 (ID180831), for evaluating the reproducibility of the effects of the moisture barrier. The flattening layer of sample 2 was successfully formed on the substrate, while a small portion of the flattening layer of sample 1 was removed from the substrate because the CFRP substrate repelled the gel used for forming the flattening layer. Figure 1 shows a picture of sample 2. Figure 2 displays a thickness measurement of the flattening layer. This figure was obtained by using the OLS4000 three-dimensional (3-D) Laser Measuring Microscope (Olympus Co. Ltd.), which has the capability to measure multiple layers of transparent material. As the flattening layer on the CFRP substrate is transparent, we can measure the surface of both the flattening layer and the carbon fibers in CFRP. We estimated the thickness of the flattening layer as a few micrometers through this measurement. Note that the SiO_x coating is so thin that we cannot recognize it in this measurement. The surface roughness of the substrate after SiO_x coating was measured to be a few tens of nanometers with a low-frequency cutoff (cutoff wavelength = 80 μm) by using OLS4000.

3 Moisture Absorption

3.1 Test of Moisture Absorption

The CFRP mirror will experience moisture absorption due to the humid air during storage on the ground even if the mirror is used in space. Thus, the moisture absorption on the ground should be minimized to reduce the deformation of the CFRP substrate. Since a low water transmissivity was expected due to the water barrier layer on the CFRP, we performed accelerated moisture absorption tests on the flat CFRP substrate at 60℃ and a relative humidity (RH) of 100%. The absorption rate was estimated to be ∼180 times that in a laboratory environment.[31] The following test procedure was employed.

1. The sample was dried in a thermal vacuum environment for 72 h at 60℃.

2. The weight [W_d in Eq. (1)] of the sample under the dried condition was measured.
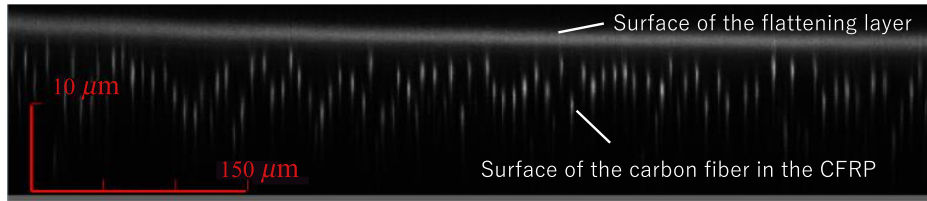
Fig. 2 Thickness measurement of the flattening layer obtained using a 3-D laser measuring microscope. This is a type of cross-sectional view of the CFRP with the flattening layer, although the bright part in this panel displays the surface viewed from above.

3. The sample was exposed to the moist environment at 60°C and an RH of 100%.

4. The weight [W_w in Eq. (1)] of the sample was measured.

5. Steps (3) and (4) were repeated.

The weight was measured with the electric balance HJ-320 produced by Shinko Denshi Co. Ltd. The repeatability of the measurement is 0.001 g. In step (3), the sample was placed in a closed container during the test. In the container, the sample was mounted above the surface of a pool of deionized water. The container was placed in an isothermal oven, following which the inside of the container was conditioned to an RH of 100% at 60°C. In step (4), the sample had moisture on the surface immediately after taking it out of the container. Therefore, we wiped the moisture and waited a few minutes for the sample to cool to the laboratory temperature. It took ∼5 to 10 min to measure the weight, which is considered as lost time in the estimation of duration.

The moisture content M of the sample was estimated as

$$M(\%) = \frac{W_w - W_d}{W_d} 100. \quad (1)$$

Figure 3 shows the time profiles of moisture content. For determining the effect of the moisture barrier, we also plotted the time profile of a sample without a moisture barrier (no coating in Fig. 3). This time profile is quoted from a previous report.[31] As expected, the moisture absorption rates of samples
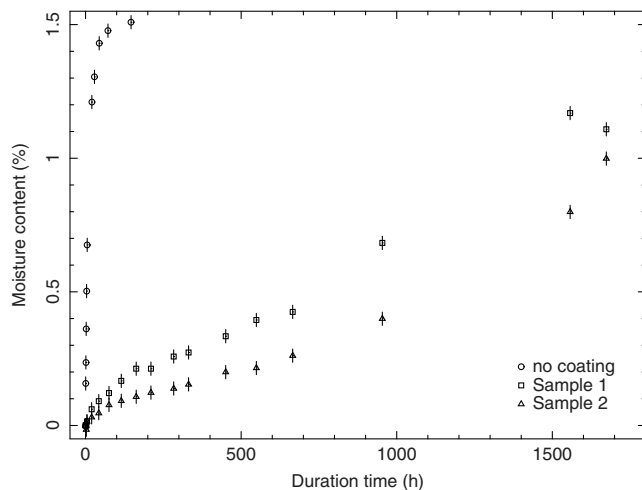
1 and 2 are less than that without the moisture barrier and the moisture content of sample 1 is greater than that of sample 2. This is caused by the defect of the flattening layer, as mentioned in Sec. 2.2. The absorption rate increases after a duration of ∼800 h. Around a duration of 600 h, cracks on the moisture barrier were observed in both samples 1 and 2. In sample 1, we observed another type of damage—specifically, circular damage on the moisture layer around a duration of 100 h—and the number of circular damage patterns increased with time. The circular damage consists of many small lumpy structures (see Fig. 4). The 3-D measurement of the circular damage indicates that the small lumpy structure is caused by the detachment of the moisture barrier from the substrate. The detachment is likely the result of weak attachment of the flattening layer of sample 1, owing to the water repelling.

3.2 Evaluation of Moisture Barrier

It is known that the diffusion of moisture in CFRP follows Fick's law.[32,33] The moisture content with respect to time is expressed as

$$M(t) = M_m \cdot 4\sqrt{\frac{Dt}{\pi h^2}}, \quad \frac{Dt}{h^2} \le 0.05,$$

$$M(t) = M_m \cdot \left[1 - \frac{8}{\pi^2} \exp\left(\frac{-\pi^2 Dt}{h^2}\right)\right], \quad \frac{Dt}{h^2} > 0.05, \quad (2)$$

where D is the diffusivity of CFRP, h is the thickness of CFRP, and M_m is the saturated moisture content. We previously pointed out that the time profiles of moisture content with a moisture barrier were not well fitted with a simple diffusion model, because the damage of the moisture barrier induced an increase in the moisture absorption.[31] As expected, the time profiles in Fig. 3 were not well fitted with the simple model, and damage to the barrier was observed. Therefore, we propose a modified model that considers the damage.

We assume that the increase rate of the damage area is proportional to the current damage area. The undamaged area A is expressed as

$$\frac{dA}{dt} = -\alpha A.$$

The damage area is deduced to be $A_m[1 - \exp(-\alpha t)]$, where A_m is the total area of the substrate. Because a CFRP substrate is so thin that the timescale for moisture to diffuse in the thickness direction is smaller than that for damage to progress, the moisture content is considered to be virtually proportional to the damage area. Thus, the moisture content, $M_d(t)$, caused by the damage is expressed as $M_d(t) = M_{dm}[1 - \exp(-\alpha t)]$, where M_{dm} is the saturated moisture content caused by damage. As the

Fig. 3 Time profiles of moisture content with respect to duration in units of hours.
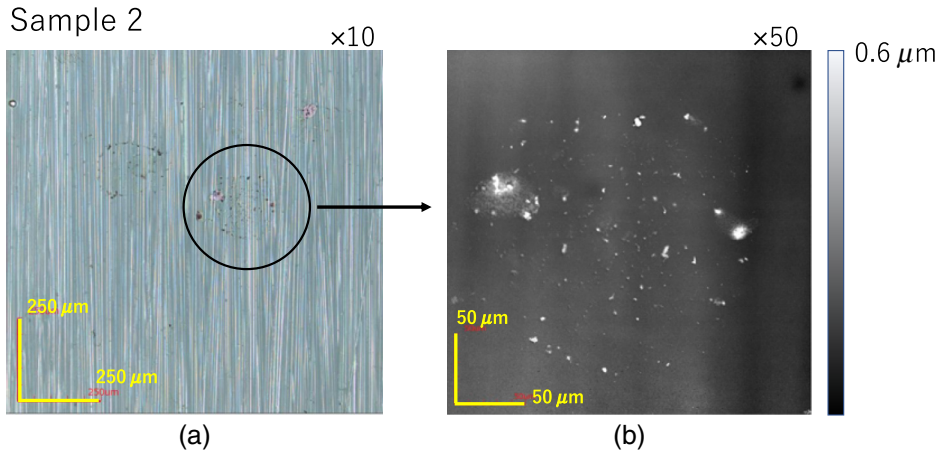
Sample 2

Fig. 4 Circular damage observed in sample 2 after the moisture absorption test. (a) Color image of the circular damage and (b) 3-D image of the circular region in (a).

damage was observed at a duration of ~600 h, it is considered that a threshold (t_{th}) exists in the duration at which moisture absorption is affected by the damage. Thus, the equation of $M_d(t)$ should be modified as

$$M_d(t) = M_{\text{dm}}\{1 - \exp[-\alpha(t - t_{\text{th}})]\}, \quad t > t_{\text{th}}. \quad (3)$$

There is an upper limit on the moisture content, which is equal to the sum of the upper limits of Eqs. (2) and (3). The increase in the moisture content resulting from the damage causes a decrease in components from diffusion. The effect is taken into account by resetting $M_m = M_{\text{up}} - M_d(t)$ and $M_{\text{dm}} = M_{\text{dm}} - M(t)$ in Eqs. (2) and (3), where M_{up} is the upper limit of moisture content.

We fitted our data with the proposed model. In the fitting, we fixed M_{up} at 1.5%, which is the saturated value in the sample without the coating. The best-fit parameters are listed in Table 2, and the best-fit curves are shown in Fig. 5. The dotted and dashed lines in Fig. 5 display the moisture content resulting from diffusion and damage, respectively. The time profiles are well fitted with this model with a reduced χ^2 of ~1.2. The diffusivity D of the coated samples is ~1/500 times that of the sample without the coating. Furthermore, the diffusivity of the coated samples is less than that of the moisture barrier film samples and virtually equal to that of the cocured sample with Super-Inver foil in our previous report (2.10×10^{-6}).[31] This result indicates that the moisture barrier works well. The small diffusivity of the order of 10^{-6} is caused by the absence of a

barrier coating on the side of the CFRP substrates, and the difference between samples 1 and 2 is attributed to the deficit of the flattening layer of sample 1. The fitting results indicate that the damage properties of sample 1 are consistent with those of sample 2, although there are many circular damage patterns in sample 1. It is likely that the barrier layer in the circular damage region detached from the substrate while maintaining similar barrier performance to that of sample 2. If the method of forming the barrier layer is similar, it will exhibit the same performance.

4 Summary and Conclusions

We have evaluated the performance of the SiO_x barrier coating on the thin CFRP substrate. In the moisture absorption test, under a condition of 60°C and an RH of ~100%, the acceleration rate was estimated to be ~180 times that in the laboratory environment. We obtained a high barrier performance equivalent to that with the Super-Inver foil reported previously, while the rate of moisture absorption increased at a duration of ~800 h, which corresponds to 16 years in the laboratory environment. The diffusivity of the samples with a barrier was only ~1/500 times that of the sample without a barrier. Cracks on the barrier layer of both samples 1 and 2 were observed at ~600 h, and the number of damages increased with time. Thus, we consider that the increase of the moisture content could be induced by these damages.

To evaluate the effect of the moisture barrier, the time profile of the moisture content should be modeled accurately. We proposed a modified model that considers the damage to the moisture barrier, instead of the simple diffusive model based on Fick's law. The observed time profile was well fitted with the proposed model. The time profile of the moisture content caused by damage was characterized in the model with α of ~10^{-3} h^{-1} and t_{th} of ~800 h. The time profile of sample 1 was virtually identical to that of sample 2. If the method of forming the barrier layer is similar, it will exhibit the same performance.

The formation of the barrier layer on the CFRP will suppress the deformation of the CFRP products due to the change in humidity so that it leads to the opening of the application of CFRP mirrors to the astronomical field. This barrier technology will be useful for x-ray mirrors that require a long-term stability in space. In our development of the CFRP mirror, the dimension stability of the CFRP mirror will be evaluated.
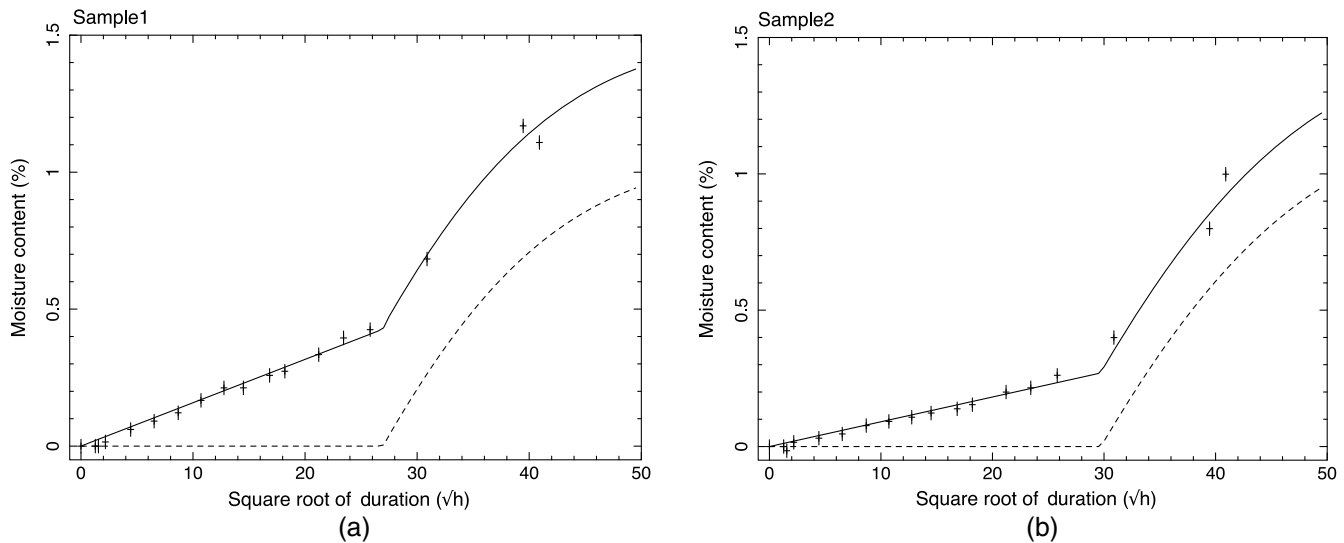
Table 2 List of best-fit parameters.

	D ($\times 10^{-6}$ mm^2 h^{-1})	α ($\times 10^{-4}$ h^{-1})	t_{th} (h)	M_{up}	χ^2/degree of freedom
Sample 1	3.50 ± 0.83	12.5 ± 3.6	730 ± 200	1.5% (fix)	15.6 (15)
Sample 2	1.15 ± 0.24	9.5 ± 1.1	883 ± 72	1.5% (fix)	18.8 (15)
No coating	968 ± 32	—	—	1.5% (fix)	—

Note: errors: 1σ level.

Fig. 5 Moisture contents of (a) sample 1 and (b) sample 2. Because the moisture content is a function of the square root of duration in Fick's law, we plot the data as a function of the square root of duration. The dotted and dashed lines represent the moisture content resulting from diffusion and damage, respectively.

Acknowledgments

References

1. L. V. Speybroeck, "Einstein observatory (HEAO-B) mirror design and performance," *Proc. SPIE* **0184**, 2–11 (1979).
2. B. Aschenbach, "Design, construction, and performance of the ROSAT high-resolution x-ray mirror assembly," *Appl. Opt.* **27**, 1404–1413 (1988).
3. M. C. Weisskopf et al., "An overview of the performance and scientific results from the Chandra x-ray observatory," *Publ. Astron. Soc. Pac.* **114**, 1–24 (2002).
4. P. J. Serlemitsos et al., "The x-ray telescope onboard ASCA," *Publ. Astron. Soc. Jpn.* **47**(1), 105S–114S (1995).
5. P. J. Serlemitsos et al., "The x-ray telescope onboard Suzaku," *Publ. Astron. Soc. Jpn.* **59**(sp1), S9–S21 (2007).
6. T. Takahashi et al., "The ASTRO-H x-ray observatory," *Proc. SPIE* **8443**, 84431Z (2012).
7. H. Awaki et al., "The hard x-ray telescopes to be onboard ASTRO-H," *Appl. Opt.* **53**, 7664–7676 (2014).
8. D. de Chambure, R. Laine, and K. van Katwijk, "X-ray telescopes for the ESA XMM spacecraft," *Proc. SPIE* **3444**, 313–326 (1998).
9. G. Boella et al., "BeppoSAX, the wide band mission for x-ray astronomy," *Astron. Astrophys. Suppl. Ser.* **122**, 299–307 (1997).
10. D. N. Burrows et al., "The swift x-ray telescope," *SpaceSci. Rev.* **120**, 165–195 (2005).
11. L. Arcangeli et al., "The eROSITA x-ray mirrors: technology and qualification aspects of the production of mandrels, shells and mirror modules," *Proc. SPIE* **10565**, 105652M (2017).
12. F. A. Harrison et al., "The nuclear spectroscopic telescope array (NuSTAR) high-energy x-ray mission," *Astrophys. J.* **770**, 103 (2013).
13. M. Bavdaz et al., "Development of the ATHENA mirror," *Proc. SPIE* **10699**, 106990X (2018).
14. F. Öze and A. Vikhlinin, "Lynx interim report," 2018, https://wwwastro .msfc.nasa.gov/lynx/docs/LynxInterimReport.pdf.
15. S. Sugita et al., "Studies of lightweight x-ray telescope with CFRP," *Proc. SPIE* **9144**, 914447 (2014).
16. T. Iwase et al., "Development of the next generation x-ray telescope using CFRP as a substrate," in *Suzaku-MAXI: Expanding the Frontiers of the X-Ray Universe*, Vol. 1, p. 160 (2014).
17. H. Awaki et al., "Development of a lightweight x-ray mirror using thin carbon-fiber-reinforced plastic (CFRP)," *Proc. SPIE* **10699**, 106993R (2018).
18. L. Wei et al., "Design and optimization of the CFRP mirror components," *Photonic Sens.* **7**, 270–277 (2017).
19. P. B. Willis and D. R. Coulter, "Durability and reliability of lightweight composite mirrors for space optical systems," *Proc. SPIE* **1993**, 127–136 (1993).
20. M. E. L. Jungwirth et al., "Large-aperture active optical carbon fiber reinforced polymer mirror," *Proc. SPIE* **8725**, 87250W (2013).
21. C. C. Wilcox et al., "Closed-loop performance of an actuated deformable carbon fiber reinforced polymer mirror," *Proc. SPIE* **8373**, 83730S (2012).
22. S. Kendrew and P. Doel, "Development of a carbon fiber composite active mirror: design and testing," *Opt. Eng.* **45**(3), 033401 (2006).
23. P. Doel et al., "Development of an active carbon fiber composite mirror," *Proc. SPIE* **5490**, 1526–1533 (2004).
24. M. E. L. Jungwirth et al., "Actuation for carbon fiber reinforced polymer active optical mirrors," in *Proc. IEEE Aerosp. Conf.*, Big Sky, Montana, pp. 1–9 (2012).
25. Y. Arao et al., "Analysis of time-dependent deformation of a CFRP mirror under hot and humid conditions," *Mech. Time-Depend. Mater.* **13**(2), 183–197 (2009).
26. R. C. Romeo and R. N. Martin, "Progress in 1m-class, lightweight, CFRP composite mirrors for the ULTRA telescope," *Proc. SPIE* **6273**, 62730S (2006).
27. S. Utsunomiya, T. Kamiya, and R. Shimizu, "Development of CFRP mirrors for space telescopes," *Proc. SPIE* **8837**, 88370P (2013).
28. J. R. Andrews et al., "Prototype 0.4 meter carbon fiber reinforced polymer (CFRP) telescope: specifications and initial testing," *Proc. SPIE* **7018**, 70184D (2008).
29. R. Börret, H. Glatzel, and M. Shmidt, "Manufacturing technologies for high throughput imaging x-ray telescopes: XMM CFRP

technology compared to the x-ray systems," *Proc. SPIE* **2210**, 348–359 (1994).

30. S. Sugita et al., "Studies of print-through and reflectivity of x-ray mirrors using thin carbon-fiber-reinforced plastic," *J. Astron. Telesc. Instrum. Syst.* **2**(1), 014002 (2016).

31. S. Sugita et al., "Studies of the moisture absorption of thin carbon fiber reinforced plastic substrates for x-ray mirrors," *J. Astron. Telesc. Instrum. Syst.* **1**(3), 034003 (2015).

32. J. Trigo, "Dimensional stability characterisation of carbon fiber with epoxy and cyanate ester resin laminates due to moisture absorption," *Spacecr. Struct. Mater. Mech. Eng.* **386**, 371–376 (1996).

33. A. C. Loos and G. S. Springer, "Moisture absorption of graphite-epoxy composites immersed in liquids and in humid air," *J. Compos. Mater.* **13**, 131–147 (1979).

Biographies of the authors are not available.